Compact double-bunch x-ray free electron lasers for fresh bunch self-seeding and harmonic lasing

C. Emma,[1] Y. Feng,[2] D. C. Nguyen,[3] A. Ratti,[2] and C. Pellegrini[1,2]
[1]*University of California, Los Angeles, California 90095, USA*
[2]*SLAC National Accelerator Laboratory, Menlo Park, California 94025, USA*
[3]*Los Alamos National Laboratory, Los Alamos, New Mexico 87545, USA*
(Received 8 December 2016; published 3 March 2017)

This paper presents a novel method to improve the longitudinal coherence, efficiency and maximum photon energy of x-ray free electron lasers (XFELs). The method is equivalent to having two separate concatenated XFELs. The first uses one bunch of electrons to reach the saturation regime, generating a high power self-amplified spontaneous emission x-ray pulse at the fundamental and third harmonic. The x-ray pulse is filtered through an attenuator/monochromator and seeds a different electron bunch in the second FEL, using the fundamental and/or third harmonic as an input signal. In our method we combine the two XFELs operating with two bunches, separated by one or more rf cycles, in the same linear accelerator. We discuss the advantages and applications of the proposed system for present and future XFELs.

DOI: 10.1103/PhysRevAccelBeams.20.030701

I. INTRODUCTION

Harmonic lasing can be used to extend the wavelength range of free electron lasers (FELs), or to reduce the electron beam energy for the same x-ray wavelength, making the accelerator system more compact [1–3]. Fresh bunch self-seeding improves the longitudinal coherence and increases the x-ray free electron laser (XFEL) peak power using a shorter undulator compared to regular self-seeding [4,5]. In this paper we present a method to achieve both goals using the compact double-bunch XFEL [6,7]. The scheme is equivalent to having two separate XFELs in succession. The first FEL uses one electron bunch to reach the saturation regime and generate a high power self-amplified spontaneous emission (SASE) x-ray pulse at the fundamental and the third harmonic [8]. The x-ray pulse is then filtered through a monochromator and seeds a different electron bunch in the second FEL, using the fundamental or third harmonic as the input signal. In our study we combine the two XFELs operating with two bunches in the same linear accelerator separated by one or more rf cycles, making the bunches lase in sequence in two different parts of the same undulator. Selective lasing with one of the two bunches is achieved by putting one bunch on an oscillating orbit around the undulator axis while placing the other bunch on axis. We note that various schemes for harmonic lasing and harmonic self-seeding have been discussed previously by other authors, and specifically, that harmonic lasing has recently been demonstrated at EUV wavelengths at the FLASH2 facility [2,9,10]. We discuss the advantages of the proposed method compared to existing schemes and its applications for present and future XFELs.

Harmonics of the fundamental are generated in FELs in a planar undulator through the process of nonlinear harmonic generation (HG), which has been successfully measured down to x-ray wavelengths [11,12]. The intensity of nonlinear harmonics however is quite low, and the longitudinal coherence is worse than regular SASE at the fundamental wavelength. An alternative approach, harmonic lasing, drives the FEL instability at the harmonic wavelength and is able to achieve higher power with narrower bandwidth and improved shot-to-shot stability [2,13]. In a single-pass FEL amplifier, harmonic lasing can reach high intensity if the gain at the fundamental wavelength is continuously disrupted such that the increase in electron slice energy spread does not halt the growth of the harmonic. This is typically achieved by introducing periodic spectral filters or phase shifters in the undulator system and has been previously studied in detail (see e.g. Refs. [2,14,15]). In a self-seeded FEL, the output intensity on the fundamental and harmonics is also limited by the electron slice energy spread increase if the lasing in the SASE section before the monochromator is taken near to the saturation level.

In this paper we show that the electron slice energy spread constraints can be overcome by generating a fundamental and/or harmonic seed with one bunch and using a second, fresh electron bunch to amplify the fundamental or harmonic radiation in a downstream undulator. A schematic of the double-bunch XFEL is shown in Fig. 1. In the first undulator, the first bunch moves on axis

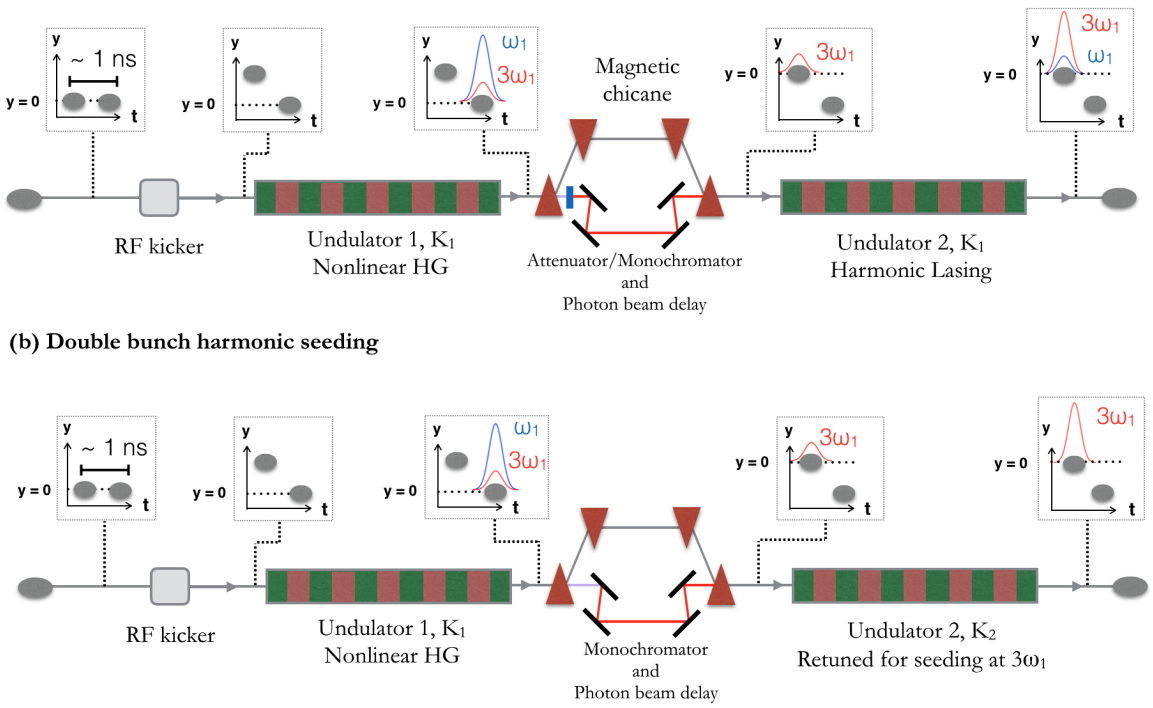

FIG. 1. Schematic of a double bunch XFEL for harmonic lasing and/or fresh bunch self-seeding. The first undulator section generates the fundamental and, through nonlinear harmonic generation, the third harmonic. The radiation is passed through a monochromator and/or attenuator to transmit the desired harmonic and attenuate the other, and to delay the x-ray pulse to temporally overlap with the second fresh electron bunch. (a) The monochromatic fundamental and/or the attenuated third harmonic is amplified by a second fresh electron bunch in the downstream undulator section. (b) The monochromatic third harmonic is amplified by a second fresh bunch in the downstream undulator retuned such that the third harmonic is the new fundamental frequency.

and generates the seeding signal, while the second bunch is put on a trajectory which oscillates around the axis by an rf kicker and does not lase. In the second undulator, after the attenuator/monochromator, the situation is inverted, the second bunch is put back on axis by appropriate dipole kicks and the first bunch oscillates around the axis. An oscillating trajectory increases the lasing gain length according to the formula [16],

$$L_g = \frac{L_{g0}}{1 - \theta^2/\theta_c^2}, \tag{1}$$

where L_{g0} is the gain length in the absence of oscillation, θ is the angular kick and $\theta_c = \sqrt{\lambda/L_{g0}}$ is the critical angle for which all lasing is suppressed. The critical angle is in the range of 10–15 μrad for 4–12 keV photon energies and typical XFEL electron beam parameters (see Table I). The main advantage of this method is that it allows the generation of a strong fundamental and harmonic seed by driving the FEL to saturation in the first SASE section. The strong seed is then amplified efficiently to high power in a short undulator section downstream. This increases the capability for harmonic XFELs beyond previous schemes [2,9,10] and opens the door for cascaded monochromatic self-seeding at higher harmonics in the future [17]. We note that at the LCLS, a version of the double-bunch FEL using two different electron slices on the head and tail of the same bunch has already been experimentally demonstrated and has been used to generate multicolor XFEL pulses as well as fresh slice self-seeded pulses with duration below 10 fs [4,18]. The double bunch XFEL is similar to the "fresh-slice" scheme of Refs. [4,18] in that it uses fresh electrons to amplify a strong seed signal [19]. The difference between our scheme and the fresh-slice approach is

TABLE I. 1D simulation parameters for the ideal double bunch XFEL. The parameters are similar to those of LCLS.

Parameter	Value
Beam energy	11.1 GeV
Peak current	3000 A
Relative energy spread	$\rho/20$
Beta function	5 m
Fundamental photon energy	5.5 keV
Undulator period	3 cm
Undulator parameter K (rms)	2.47
FEL parameter ρ [$\times 10^{-3}$]	0.7
1D gain length $L_g^{(1)}$	2 m

that we use an rf kicker instead of a dechirper to provide the transverse deflection. Passive transverse deflection using a dechirper has the disadvantages of inducing emittance and energy spread growth on the deflected bunch slices, as well as a time-dependent focusing from the quadrupole components of the wakefield [20,21]. The double-bunch XFEL has the advantage that the entire electron bunch lases in the second undulator, increasing the total energy of the x-ray pulse. We also note that two bunches with ns separation have been produced at LCLS and used to deliver x-ray pulses with ns delay to user experiments [22].

The paper is structured as follows. In Sec. II we discuss the theory of harmonic XFELs highlighting the relevant scaling laws and placing emphasis on the impact of the electron slice energy spread. In Sec. III we study the double-bunch harmonic XFEL in the 1D limit and present simulation results for an idealized case. We also present 1D simulations for an advanced gradient undulator (AGU) designed to achieve the largest gain in the shortest distance [5]. In Sec. IV we show results from 3D FEL simulations using the AGU and the double bunch XFEL with monochromatic seeding. In Sec. V we discuss the monochromator/attenuator system providing the x-ray delay to overlap the seed on the second bunch. In Sec. VI we discuss the system used to generate oscillations for the first and second electron bunches around the undulator axis. In conclusion, we discuss possible applications of this method in existing and future XFELs.

II. THEORY

In a double bunch harmonic XFEL the electron bunch generates and amplifies harmonic radiation via two separate processes: nonlinear HG and harmonic lasing. Nonlinear HG arises from the harmonic components of the electron beam bunching due to interaction with the fundamental wavelength, and becomes significant only when the fundamental radiation is near saturation. The fundamental therefore dominates the FEL process in the first nonlinear HG section and determines the electron beam evolution and properties at the exit of the first undulator (see Fig. 1). In the cold beam limit $\sigma_\gamma \ll \rho$, where ρ is the FEL parameter, we can neglect the initial electron slice energy spread. In this limit nonlinear HG produces ~2%–3% of the fundamental power at the third harmonic at saturation, where the electron beam slice energy spread increases to $\sigma_\gamma \sim \rho$. The statistical properties of nonlinear HG starting from shot noise show that the SASE radiation is less longitudinally coherent and the shot-to-shot intensity fluctuations are larger for the third harmonic than the fundamental [23].

Increasing the power and improving the longitudinal coherence of harmonic emission is achieved via harmonic lasing in the second section of the two-stage system. In conventional harmonic lasing the electron bunch amplifies the harmonic seed signal while the fundamental growth is disrupted via spectral/phase filters so that it remains significantly lower than the harmonic. The separation between spectral/phase filters is determined by the gain length ratio between the hth harmonic and the fundamental which in the cold beam limit is given by $L_{gh}/L_{g1} = ([JJ]_h^2/h[JJ]_1^2)^{1/3}$ [24]. The Bessel factors are defined as $[JJ]_h = (-1)^{(h-1)/2} * [J_{(h-1)/2}(h\xi) - J_{(h+1)/2}(h\xi)]$ where $\xi = K^2/(4+2K^2)$ and K is the peak undulator parameter.

Assuming lasing at the fundamental is adequately suppressed the saturation power at the hth harmonic is around $1/h$ times the fundamental power, an order of magnitude increase compared to nonlinear HG. Furthermore, since the slippage in harmonic lasing is determined by the fundamental, the longitudinal coherence and the spectral brightness of the hth harmonic increases by a factor h compared to the fundamental [25,26], giving the same brightness for the fundamental and harmonics.

A. Warm beam effects

As discussed in Refs. [2,24] the success of harmonic lasing schemes critically depends on the electron beam parameters, particularly the electron slice energy spread. An estimate of the desired beam quality is obtained by requiring that the wavelength spread due to electron slice energy spread be smaller than the spectral linewidth at saturation. From this we obtain the energy spread constraint for efficient harmonic lasing $\sigma_\gamma < \rho/h$ [24]. In the case of third harmonic lasing, Ref. [24] shows that increasing the energy spread beyond the desired value ($\sigma_\gamma \to \rho/3$) significantly increases the saturation length and reduces the saturation power below $\rho P_{\mathrm{beam}}/h$ in the 1D limit. In 3D theory, a generalized solution of the eigenvalue equation for high gain FELs including harmonics and all relevant three-dimensional effects was presented in Refs. [2,27]. From Ref. [2] we obtain expressions for the three-dimensional gain length for both the fundamental $L_g^{(1f)}$ and third harmonic $L_g^{(3h)}$ and plot the ratio of these in Fig. 2 for a typical hard x-ray set of parameters (see Table I). As is shown clearly in the figure, the gain length ratio increases rapidly with increasing slice energy spread while it is less sensitive to changes in the beam current. It is important to note that for harmonic lasing the ratio is inversely proportional to the "catch-up distance" before the fundamental approaches the third harmonic power and harmonic lasing is disrupted. Using a fresh bunch/slice of electrons in a two-stage harmonic XFEL allows the third harmonic to reach saturation $P_3 \sim \rho P_{\mathrm{beam}}/3$ [1] before the fundamental takes over the FEL process. This can be achieved using a single spectral filter, relaxing the requirements on hardware compared to typical harmoniclasing schemes.

III. 1D NUMERICAL EXAMPLES

In the framework of the 1D theory of FELs neglecting slippage, betatron motion and diffraction of radiation, the

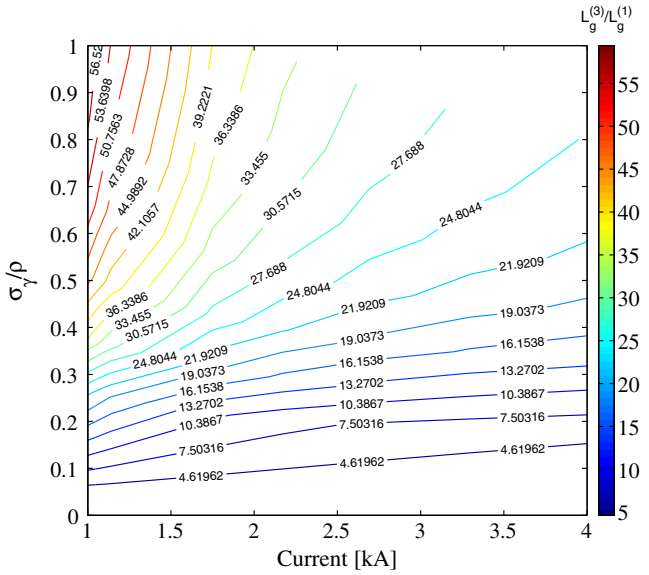

FIG. 2. Gain length ratio between the third harmonic and the fundamental assuming the beta function is optimized for third harmonic lasing and the parameters are those in Table I. At large energy spread values $\sigma_\gamma > \rho/3$ the third harmonic gain length is over 10 times the fundamental for all values of the beam current. This prohibits efficient harmonic lasing without the frequent use of phase shifters or attenuators to disturb the fundamental gain.

equations governing the evolution of a two-frequency system (fundamental and third harmonic) can be written as follows [1,24]:

$$\frac{d\theta_j}{dz} = k_w \times \left(1 - \frac{\gamma_r^2}{\gamma_j^2}\right) \tag{2}$$

$$\frac{d\gamma_j}{dz} = -\frac{\chi_1}{\gamma_j} * \Re\{K_1 E_1(z) e^{i\theta_j} + K_3 E_3(z) e^{3i\theta_j}\} \tag{3}$$

$$\frac{dE_1}{dz} = -\chi_2 K_1 \langle \frac{e^{i\theta_j}}{\gamma_j} \rangle \tag{4}$$

$$\frac{dE_3}{dz} = -\chi_2 K_3 \langle \frac{e^{3i\theta_j}}{\gamma_j} \rangle, \tag{5}$$

where we define $\chi_1 = e/2m_e c^2$ and $\chi_2 = I/8\pi\epsilon_0 c\sigma_e^2$, the resonant energy $\gamma_r^2 = \lambda_w/2\lambda_s(1 + K^2/2)$ and $K_h = K * [JJ]_h$ is the harmonic coupling which decreases for higher harmonic number h. The complex electric fields E_1 and E_3 represent the fundamental and third harmonic. We integrate Eqs. (1)–(4) using the parameters in Table I to simulate a double-bunch harmonic lasing XFEL (see Fig. 3). In our ideal case we assume the attenuator (located at $z/L_{g1} = 21$) completely transmits the third harmonic and eliminates the fundamental. We consider the cold beam limit $\sigma_\gamma/\rho = 1/20$. The first undulator section generates

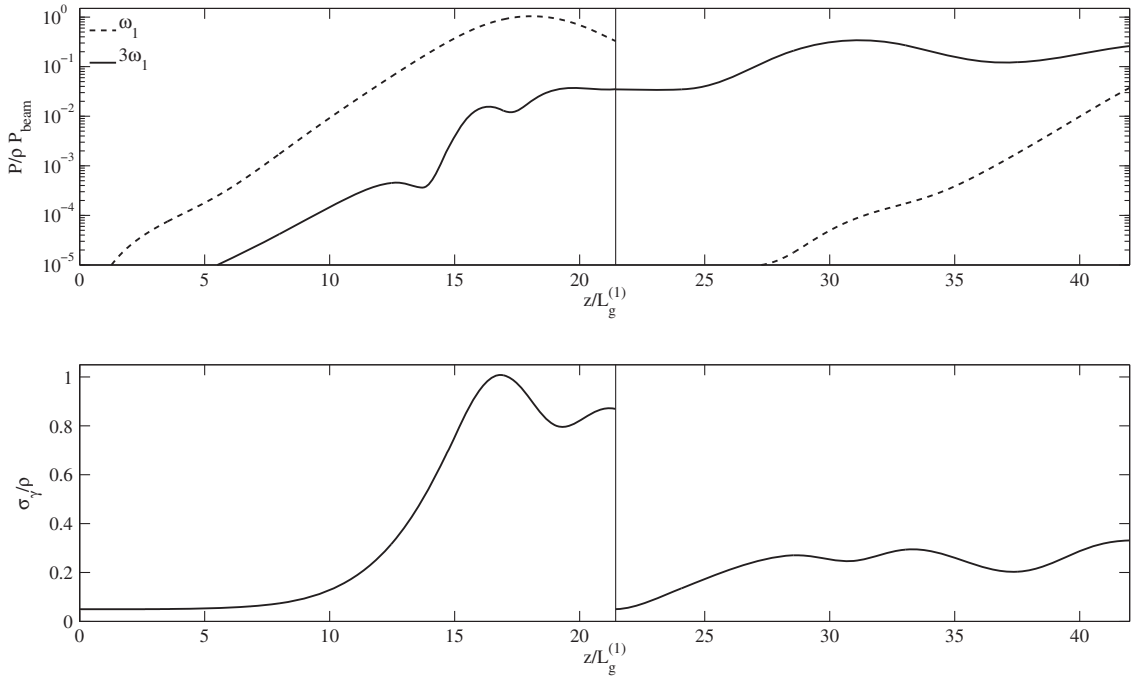

FIG. 3. 1D simulation of the ideal double bunch XFEL. The parameters are those in Table I, the simulation assumes an attenuator at $z/L_{g1} = 21$ which transmits the third harmonic and completely absorbs the fundamental. The radiation power is normalized to the fundamental saturation power ρP_{beam}. In the second undulator, the third harmonic power and energy spread grow to about 1/3 of the power and energy spread at the fundamental saturation.

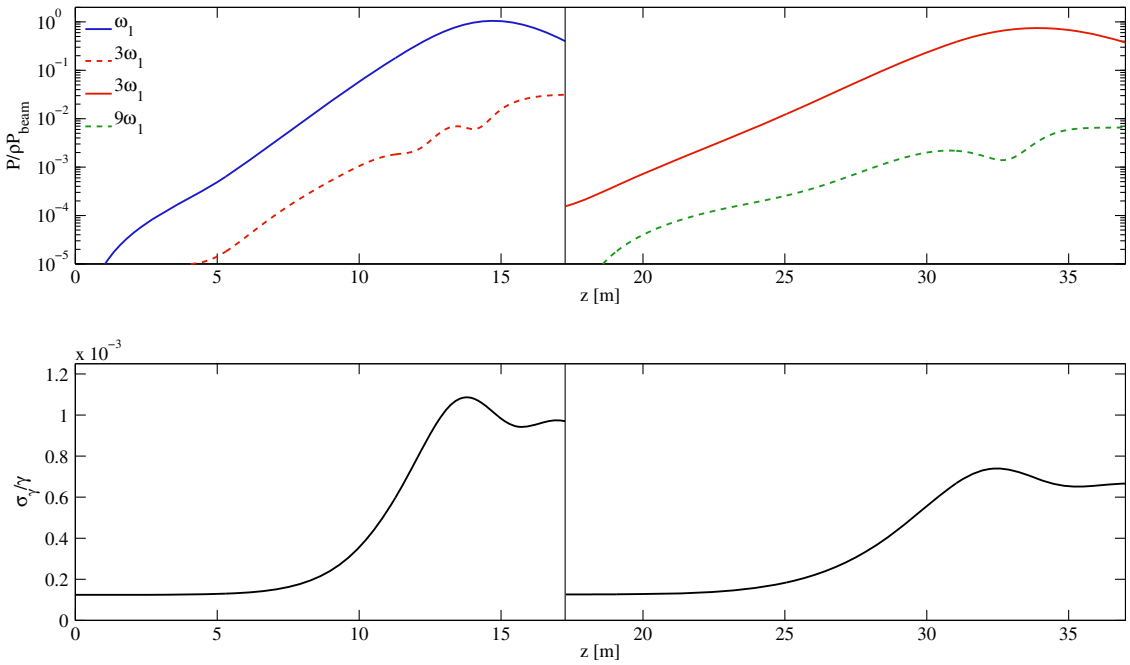

FIG. 4. 1D simulation of the double bunch harmonic XFEL with monochromatic seeding and a retuned second undulator. The parameters are those in Table I, the simulation assumes a monochromator at $z = 17$ m which transmits 0.5% of the third harmonic and completely blocks the fundamental. The radiation power is normalized to the fundamental saturation power ρP_{beam}. The solid lines represent lasing at the fundamental wavelength before/after the attenuator, the dashed lines represent lasing via harmonic generation.

radiation at the fundamental and at the third harmonic via nonlinear HG. The third harmonic saturates at 3.5% of the fundamental power around $z/L_{g1} = 19$. We assume the seed from nonlinear HG is perfectly overlapped with fresh electrons in the second undulator section and drives harmonic lasing. Harmonic lasing saturates in about eight gain lengths after the attenuator in the second section, with 34% of the beam power in the third harmonic, agreeing well with expectation from theory. We note that at the second saturation point the fundamental power is 4 orders of magnitude smaller than the third harmonic. We now consider 1D simulations of double bunch harmonic seeding using an advanced gradient undulator (AGU) [5], with the second undulator section retuned so the fundamental is resonant with the third harmonic generated in the first section [see Fig. 1(b)]. The advantages of retuning the second undulator section are threefold: first, there is no lasing at the ω_1 frequency that would impede the growth of the $3\omega_1$ frequency which is now the new fundamental in the second section. Furthermore, the second undulator section can be tapered to increase the third harmonic power beyond the saturation value $P_3/P_{\text{beam}} \sim \rho/3$. Finally, the nonlinear HG process in the second undulator section generates radiation at the ninth harmonic which can be used as a seed for a third section in a cascaded three-bunch configuration. The simulation parameters for the 1D AGU case are in Table II and the results are shown in Fig. 4. Note that in practice the short 5 m beta function requires short, 1 m long undulator sections with 20 cm breaks and advanced focusing [5]. The fundamental reaches the average saturation power, calculated along the entire x-ray pulse, of 40 GW after ~19 gain lengths with 1.2 GW of third harmonic content. We assume a monochromator at $z = 17$ m which transmits 0.5% of the third harmonic and completely blocks the fundamental. This efficiency is typical for diamond monochromator based self-seeding at LCLS [28]. We retune the second undulator section such that it is now resonant with $\hbar\omega_3 = 37.35$ keV and continue the simulation until saturation around z = 35 m. The saturated average power at the third harmonic is 30 GW with 260 MW of power at the ninth harmonic $\hbar\omega_9 = 112$ keV. While we have not carried out a detailed

TABLE II. Double bunch XFEL simulation parameters for the 1D AGU case. The FEL parameter and 1D gain length are for the fundamental photon energy of 12.45 keV.

Parameter	Value
Beam energy	12 GeV
Peak current	3000 A
Slice energy spread	1.5 MeV
Beta function	5 m
Normalized transverse emittance	0.15 μm
Fundamental photon energy	12.45 keV
Undulator period	2 cm
Undulator parameter K (rms)	2.12 → 0.91
FEL parameter ρ [$\times 10^{-3}$]	1.1 → 0.69
1D gain length $L_g^{(1)}$	0.82 → 1.34 m

taper optimization, preliminary simulations with a quadratic postsaturation taper and a 40 m long second section show that the third harmonic power can be increased by over a factor of 20, with 650 GW at the undulator exit.

IV. 3D SIMULATION WITH AN ADVANCED GRADIENT UNDULATOR

We now consider three-dimensional effects with a numerical example of the double bunch harmonic XFEL using the 3D FEL simulation code GENESIS [29]. The electron beam and undulator parameters are the same as those in Table II. Time dependent simulations are carried out in the retuned configuration of Fig. 1(b). The monochromator design, described in Sec. V, ensures a nearly 100% transmission after four reflections in the selected bandwidth window which in simulation is set to be 3.7 eV, a relative bandwidth $\Delta\omega/\omega_3 = 10^{-4}$. The reduction in intensity after the monochromator (see Fig. 5) is due to the narrowing of the bandwidth between incident and transmitted radiation. The number of macroparticles per slice is 2^{16} to ensure accurate resolution of the harmonic field components in the simulation [30,31]. The average radiation power is calculated for a 10 fs electron bunch and ten simulations carried out with different random initializations of the electron beam shot noise. As discussed in Ref. [2] the fluctuations are larger for the nonlinear third harmonic than for the fundamental SASE radiation at saturation ($z = 30$ m). Furthermore, the statistical fluctuation of the filtered radiation will increase up to 100% as the number of spectral modes is reduced to ~1 after the monochromator. This requires, as in a regular self-seeded FEL, that the length of the second undulator is chosen to exceed the saturation length sufficiently to suppress fluctuation of the final output power.

As shown in Fig. 5, the average power at the third harmonic (37.35 keV) at the undulator exit is more than an order of magnitude larger than what one obtains from nonlinear HG at the location of fundamental saturation ($z = 30$ m). While the first undulator section is planar to ensure efficient generation of nonlinear HG, the seeded section can be both planar or helical, with the helical undulator performing better due to the increased coupling between the electron bunch and the radiation. At saturation the seeded harmonic section reaches 10 GW at $z = 55$ m in the helical case and 7.5 GW at $z = 60$ m in the planar case, with the narrow bandwidth preserved after amplification. The 3D saturation power is in very good agreement with the typical estimated value $1.6\rho P_{\mathrm{beam}} * (L_g^1/L_g^{3D})^2$ [32]. We note that with a simple quadratic postsaturation taper (not shown) the average power at 37.35 keV exceeds 50 GW at the exit of a 75 m long undulator.

The case of fresh bunch self-seeding has been investigated via experiment and 3D simulation in previous work [4,5,33]. There it is shown that self-seeding with a fresh electron slice can increase the brightness of existing XFEL sources and increase the power of future XFELs to the multi-TW level. An advantage of the double-bunch XFEL system is the ability to increase the number of photons, since an entirely fresh electron bunch, instead of a fresh slice, is used to amplify the seed radiation downstream of the monochromator.

V. MONOCHROMATOR/ATTENUATOR SYSTEM

The design of the monochromator system for the double-bunch XFEL is shown schematically in Fig. 6, where four Bragg single crystals are arranged to form an optical chicane to select the third harmonic x-ray radiation of the upstream undulator as well as to provide the necessary and sufficient delay to allow temporal overlap with the

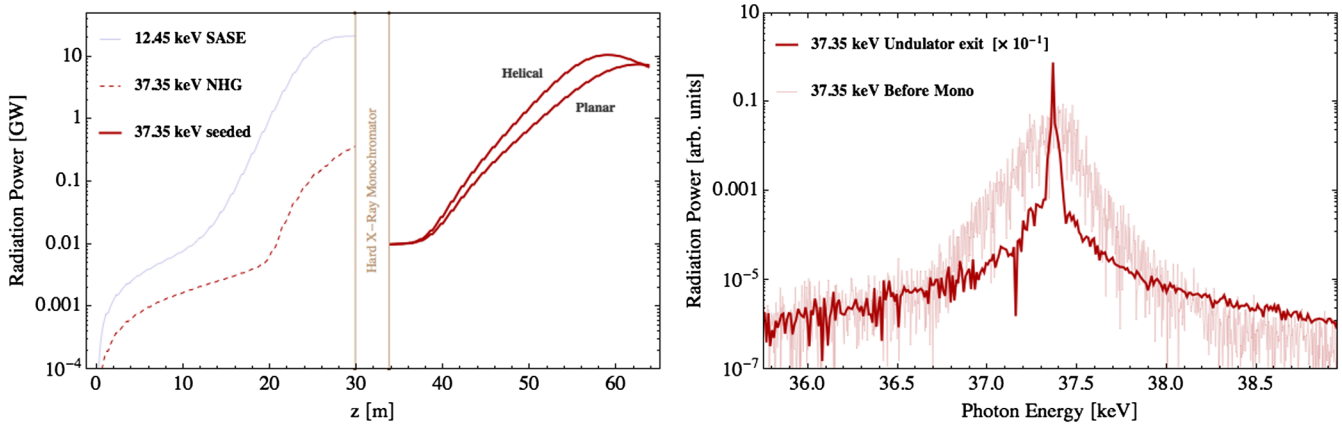

FIG. 5. 3D simulation of the double bunch harmonic XFEL with monochromatic seeding using the AGU and a retuned second undulator section. The parameters are those in Table II, except the fundamental photon energy which is tuned to 5.5 keV. The simulation assumes a four-bounce monochromator at $z = 38$ m which transmits 100% of the third harmonic and completely blocks the fundamental. The average power is calculated for a 10 fs long electron beam and ten simulations carried out with different random initializations of the electron beam shot noise. The spectrum is taken at the undulator exit and before the monochromator.

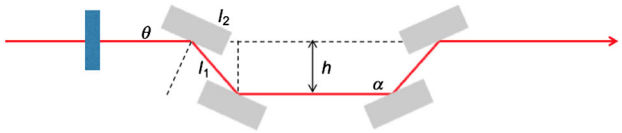

FIG. 6. Schematic of the monochromator/attenuator photon delay line for the double-bunch FEL. The delay is controllable and on the order of 1 ns to match the separation of the two bunches coming from the linac. To filter out the fundamental x-ray pulse using an attenuator (in blue), it is better to put the thin filter disk upstream of the optics to minimize the thermal load on the crystal.

second bunch. For both photon energies of the third harmonic at 16.5 and 37.35 keV, the Si (400) and diamond (400) Bragg reflections are chosen to optimize the incidence angle and the bandwidth. To minimize the footprint of the optics, a larger incidence angle is preferred, which in turn requires the use of higher order reflections [Si (400) as opposed to Si (111)] or crystals with smaller lattice constants (diamond as opposed to Si). At the same time, the same requirement will result in smaller bandwidth, which could potentially stretch the FEL pulse to beyond its original length. As such, Si (400) at 16.5 keV and diamond (400) at 37.35 keV provide reasonable compromises, although the sizes of the both optics arrangements are still rather substantial. The total time delay of the monochromator is given by $\Delta t = 2h[1 + \cos(\alpha)]/\sin(\alpha)$, where $\alpha = 2(\pi/2 - \theta)$ with θ being the Bragg angle. To generate 1 ns delay using the Si (400) at 16.5 keV, $\theta = 16.065$, and $h = 521$ mm, for diamond (400) at 37.35 keV, $\theta = 10.727$, and $h = 792$ mm accordingly. Should mechanical stability become an issue, higher order reflections could be used instead, albeit at the expense of producing even smaller bandwidths.

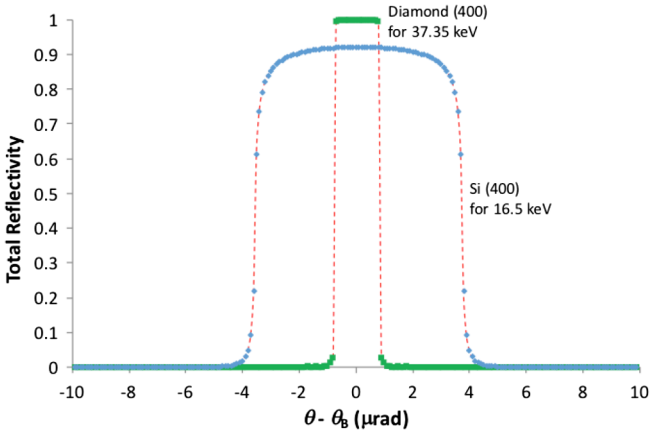

FIG. 7. Total reflectivity of the monochromator (combined four reflections) as a function of Bragg angle for two different materials at two different photon energies, Diamond (4 0 0) and Si (4 0 0) at 37.35 and 16.5 keV, respectively. The reflectivity of each reflection was obtained by using the open x-ray software toolkit XOP [34].

The combined reflectivities of monochromator for the case of Si (400) at 16.5 keV and diamond (400) at 37.35 keV are shown in Fig. 7, where $\Delta\theta$ in μrad is the deviation of the incidence angle from the Bragg angle θ_B. The combined reflectivities were calculated by convolving the reflectivities of each of the reflections from the four crystals with the two crystals of the first and the second pairs in the nondispersive configuration, and the two pairs in the dispersive configuration. The reflectivity of each reflection was obtained by using the open x-ray software toolkit XOP [34]. The combined peak reflectivity of all four crystals for Si (400) at 16.5 keV is close to 92%, whereas for diamond (400) at 37.35 keV, it is nearly 100%. To filter out the fundamental x-ray radiation using an attenuator, it is better to put the thin filter disk upstream of the optics to minimize the thermal load on the crystals so no cooling is needed on the crystals.

VI. CONTROLLED OSCILLATIONS VIA RF KICKERS

One important element of the double-bunch XFEL scheme is the ability to kick two bunches separated by approximately 1 ns in a reliable and repeatable way in order to feed the two undulator sections used in this configuration.

A. Technology choice considerations

Two conventional methods to design deflecting kickers make use of magnetic or stripline kickers or, in alternative, rf cavities [35–37]. For the novel laser scheme presented here, the choice of transverse rf electric field deflectors offers considerable advantages over stripline or ferrite based kicker options, in particular because achieving a rise time and stability in the ~1 ns bunch spacing would be particularly challenging. The selection of rf deflectors also benefits from the steady state nature of the CW transverse fields which provides higher deflection stability and shot-to-shot reproducibility when compared to those achievable with fast kickers. An additional benefit of this choice is the intrinsic ability to kick a high repetition rate beam well above the few hundred kHz limit represented by fast kickers. Furthermore, while transverse deflecting cavities are not a new discovery and have been used for beam diagnostics for many years, recent advances in rf deflectors design make it possible to leverage existing studies and develop a compact, yet effective cavity [38–41]. The ~1 ns separation between the two bunches adds however some constraints to the design of an rf kicker structure, as discussed in more detail below.

B. rf deflection

In this approach, an rf transverse deflector would provide the ~10 μrad (close to the critical angle at hard x-ray wavelengths) net deflection to the electron bunch, in a

direction dependent on the phase between the electron bunch and the rf deflector. If we consider that the transverse deflection θ_T experienced by a $\beta = 1$ electron beam during the effective length of the deflector system is given by

$$\theta_T = \frac{\Delta p_T}{p_L} \tag{6}$$

$$\Delta p_T = \Delta \int \vec{F}_T dt = \frac{e}{c} V, \tag{7}$$

where Δp_T is the transverse momentum kick, p_L is the longitudinal momentum of the beam particle, $\vec{F}_T$ is the transverse Lorentz force, and V is the transverse deflecting voltage, then it follows that a total transverse voltage of 100 kV is required to achieve 10μrad deflection for a 10 GeV beam. We note that the energy spread induced due to the finite electron beam size $\Delta\gamma/\Delta\gamma_0 \approx \phi^2/2$ with $\phi = \sigma_z/\lambda_{rf}$ where λ_{rf} is the rf wavelength and σ_z the rms bunch length, is negligible at relevant bunch lengths and rf frequencies.

C. Beam dynamics considerations

The simplest option to configure an rf deflector is that of sending the leading bunch straight when crossing the rf cavity when its field is zero, while the trailing bunch is deflected by passing through the cavity at its maximum field on crest. An important consideration is that bunches traveling at the zero-crossing phase in rf deflectors can experience transverse emittance dilution from spatial chirp [42,43]. The relative projected emittance growth is

$$\frac{\Delta\epsilon}{\epsilon_0} \approx \sqrt{1 + \left(\frac{2\pi x_0' \sigma_z}{\lambda_{rf}}\right)^2 \frac{\beta\gamma}{\epsilon_N}} - 1, \tag{8}$$

where λ_{rf} is the rf wavelength, σ_z the rms bunch length and $x_0' = eV/E_0$ the deflection at the crest. As a consequence, higher frequencies provide larger emittance growth for the same bunch length, while lower frequencies can be limited by spatial dimensions. For example, a 650 MHz rf cavity providing a 10 μrad deflection with a 15 μm rms beam size results in a negligibly small projected emittance growth $\Delta\epsilon/\epsilon_0 \approx 2 \times 10^{-7}$.

An additional requirement on the rf system is that jitter in the bunch arrival time and/or in the cavity amplitude and phase can induce unwanted deflections to the bunch centroid. The rms phase jitter tolerance at the zero crossing and the rf amplitude tolerance at the crest phase are expressed by [44]

$$\sigma_{\Delta t} \leq \frac{n_\sigma}{2\pi\nu} \frac{E_0}{\mathrm{eV}} \sqrt{\frac{\epsilon_N}{\beta\gamma}}, \qquad \frac{\sigma_V}{V} \leq n_\sigma \frac{E_0}{\mathrm{eV}} \sqrt{\frac{\epsilon_N}{\beta\gamma}}, \tag{9}$$

where E_0 is the beam energy and n_σ is the allowable rms centroid jitter in units of a fraction of the transverse rms beam size. For a maximum deflection of 10 μrad and a $n_\sigma = 5\%$ beam jitter the tolerances for phase and amplitude jitter are 2.8 ps and 1.1%, achievable in practice for state-of-the-art cavities. Lower frequencies and weaker rf kicks would minimize emittance growth and reduce phase and amplitude jitter effects. If needed, higher harmonic cavities [45] would alleviate these effects by compensating the deflecting field derivative at the zero-crossing phase.

One way to mitigate the potentially negative effects of both spatial chirp and timing jitter is to run both bunches at opposite peaks of the rf field in the cavity and configure the optical transport accordingly: in this case the effects of both the curvature of the sine wave and the jitter on the arrival timing of the ~50 fs long bunch would be minimized.

Another important limitation for ultrashort bunches so closely spaced is that wakefields created in the deflecting cavity by the leading bunch will be impacting the following one. Furthermore, since the bunches are very short, their harmonic content is very broad, which will impose tight restrictions on the allowable higher order modes. The issue of longitudinal impedance and higher order modes needs to be carefully considered in the cavity design in order to avoid undesired effects. A mitigating factor is that the relatively weak field required to deflect these bunches allows for a cavity design with a relatively low R/Q therefore alleviating in part the concern for the longitudinal wakefield of the fundamental frequency. Similarly, large higher order mode (HOM) coupler apertures will help extracting and damping HOMs.

In terms of cavity design, the bunch spacing will allow options for cavity frequencies. For example if one selected 650 MHz, a 770 ps bunch spacing would put two consecutive bunches on the two opposite crests of the cavity deflecting field. The requirements of field stability directly reflect on requirements for cavity amplitude and phase stability controls. In the case of copper cavities, stability of 10^{-4} should be within the reach of conventional controllers.

VII. CONCLUSION

In this paper we have presented a new method, the double-bunch XFEL, to obtain high power harmonic lasing, fresh bunch self-seeding and harmonic seeding at high photon energies in a compact undulator. With this method we eliminate the detrimental impact of increasing energy spread which limits the performance of conventional harmonic lasing and fundamental/harmonic seeding schemes. Furthermore, we relax the requirement on the number of spectral filters/phase shifters which are typically used to suppress the fundamental gain in harmonic lasing FELs.

Possible applications of this scheme with gap-tunable undulator could include cascaded configurations where consecutive harmonic lasing sections use the hth harmonic as the new fundamental to reach even higher photon energies. While we have not conducted a detailed tapering optimization for this kind of system, preliminary simulations suggest a quadratic postsaturation taper can be used in the harmonic

lasing system to increase the power of the third harmonic past the nominal 1D saturation value $\rho P_{\mathrm{beam}}/3$.

ACKNOWLEDGMENTS

This work was funded by the U.S. Department of Energy under Grant No. DE-SC0009983:0003. D. C. N. work at Los Alamos National Laboratory (LANL) was supported by the LANL Laboratory Directed Research and Development Program. We wish to thank Z. Huang, A. Marinelli, G. Marcus and T. Raubenheimer for many useful discussions.

[1] R. Bonifacio, L. D. Salvo, and P. Pierini, Large harmonic bunching in a high-gain free-electron laser, Nucl. Instrum. Methods Phys. Res., Sect. A **293**, 627 (1990).

[2] E. A. Schneidmiller and M. V. Yurkov, Harmonic lasing in x-ray free electron lasers, Phys. Rev. ST Accel. Beams **15**, 080702 (2012).

[3] M. J. Schmitt and C. J. Elliott, Even-harmonic generation in free-electron lasers, Phys. Rev. A **34**, 4843 (1986).

[4] C. Emma, A. A. Lutman, M. W. Guetg, J. Krzywinski, A. Marinelli, J. Wu, and C. Pellegrini (unpublished).

[5] C. Emma, K. Fang, J. Wu, and C. Pellegrini, High efficiency multi terawatt x-ray free electron lasers, Phys. Rev. Accel. Beams **19**, 020705 (2016).

[6] Y. Ding, Z. Huang, and R. D. Ruth, Two-bunch self-seeding for narrow-bandwidth hard x-ray free-electron lasers, Phys. Rev. ST Accel. Beams, **13**, 060703 (2010).

[7] G. Geloni, V. Kocharyan, and E. Saldin, DESY Report No. 10-033, 2010, https://arxiv.org/abs/1003.2548.

[8] R. Bonifacio, C. Pellegrini, and L. Narducci, Collective instabilities and high-gain regime in a free electron laser, Opt. Commun. **50**, 373 (1984).

[9] G. Geloni, V. Kocharayan, and E. Saldin, Scheme to increase the output average spectral flux of the European XFEL at 14.4 keV, in *Proceedings of the International Free Electron Laser Conference, Daejeon, Korea, 2015*.

[10] E. Schneidmiller and M. Yurkov, Studies of harmonic lasing self-seeded FEL at FLASH2, in *Proceedings of the International Particle Accelerator Conference, Busan, Korea, 2016*.

[11] E. Allaria, F. Curbis, M. Coreno, M. Danailov, B. Diviacco, C. Spezzani, M. Trovó, and G. De Ninno, Experimental Characterization of Nonlinear Harmonic Generation in Planar and Helical Undulators, Phys. Rev. Lett. **100**, 174801 (2008).

[12] D. Ratner *et al.*, Second and third harmonic measurements at the linac coherent light source, Phys. Rev. ST Accel. Beams **14**, 060701 (2011).

[13] J. Murphy, C. Pellegrini, and R. Bonifacio, Collective instability of a free electron laser including space charge and harmonics, Opt. Commun. **53**, 197 (1985).

[14] G. Marcus, Y. Ding, Z. Huang, T. Raubenheimer, and G. Penn, Report No. SLAC PUB 16081, 2014.

[15] D. Ratner, Z. Huang, W. Fawley, N. Rodes, E. Schneidmiller, M. Yurkov, and E. Allaria, Harmonic lasing at the LCLS, in *Proceedings of the International Free Electron Laser Conference, New York, USA, 2013*.

[16] T. Tanaka, H. Kitamura, and T. Shintake, Consideration on the BPM alignment tolerance in x-ray FELS, Nucl. Instrum. Methods Phys. Res., Sect. A **528**, 172 (2004).

[17] D. Nguyen, P. Anisimov, C. E. Buechler, J. Lewellen, and Q. R. Marksteiner, LANL Report No. LA-UR-15-27018, 2015.

[18] A. Lutman, T. J. Maxwell, J. P. MacArthur, M. Guetg, N. Berrah, R. Coffee, Y. Ding, Z. Huang, A. Marinelli, S. Moeller *et al.*, Fresh-slice, multicolour X-ray free electron lasers, Nat. Photonics **10**, 745750 (2016).

[19] I. Ben-Zvi, K. Yang, and L. Yu, The fresh-bunch technique in FELS, Nucl. Instrum. Methods Phys. Res., Sect. A **318**, 726 (1992).

[20] K. Bane and G. Stupakov, Dechirper wakefields for short bunches, Nucl. Instrum. Methods Phys. Res., Sect. A **820**, 156 (2016).

[21] P. Craievich and A. Lutman, Effects of the quadrupole wakefields in a passive streaker, Nucl. Instrum. Methods Phys. Res., Sect. A (to be published).

[22] F. Decker, S. Gilevich, Z. Huang, H. Loos, A. Marinelli, C. Stan, J. Turner, Z. van Hoover, and S. Vetter, Two bunches with ns-separation with LCLS, in *Proceedings of the International Free Electron Laser Conference, Daejeon, Korea, 2015*.

[23] E. L. Saldin, E. A. Schneidmiller, and M. V. Yurkov, Properties of the third harmonic of the radiation from self-amplified spontaneous emission free electron laser, Phys. Rev. ST Accel. Beams **9**, 030702 (2006).

[24] B. W. J. McNeil, G. R. M. Robb, M. W. Poole, and N. R. Thompson, Harmonic Lasing in a Free-Electron-Laser Amplifier, Phys. Rev. Lett. **96**, 084801 (2006).

[25] D. Xiang, Y. Ding, Z. Huang, and H. Deng, Purified self-amplified spontaneous emission free-electron lasers with slippage-boosted filtering, Phys. Rev. ST Accel. Beams **16**, 010703 (2013).

[26] C. Pellegrini, A. Marinelli, and S. Reiche, The physics of x-ray free-electron lasers, Rev. Mod. Phys. **88**, 015006 (2016).

[27] Z. Huang and K.-J. Kim, Three-dimensional analysis of harmonic generation in high-gain free-electron lasers, Phys. Rev. E **62**, 7295 (2000).

[28] J. Amann, W. Berg, V. Blank, F. J. Decker, Y. Ding, P. Emma, Y. Feng, J. Frisch, D. Fritz, J. Hastings *et al.*, Demonstration of self-seeding in a hard-x-ray free-electron laser, Nat. Photonics **6**, 693 (2012).

[29] S. Reiche, Genesis 1.3: A fully 3D time-dependent FEL simulation code, Nucl. Instrum. Methods Phys. Res., Sect. A **429**, 243 (1999).

[30] W. Fawley, An enhanced GINGER simulation code with harmonic emission and HDF5 IO capabilities, LBNL Technical Note, 2006.

[31] G. Marcus, W. M. Fawley, E. A. Schneidmiller, and S. Reiche, Report No. SLAC PUB 16082, 2014.

[32] K. J. Kim and M. Xie, Self-amplified spontaneous emission for short wavelength coherent radiation, Nucl. Instrum. Methods Phys. Res., Sect. A **331**, 359 (1993).

[33] C. Emma, A. Lutman, M. Guetg, A. Marinelli, J. Wu, and C. Pellegrini, Demonstration of fresh slice self-seeding in a hard x-ray free electron laser, in *Proceedings of the North*

American Particle Accelerator Conference, Chicago, USA, 2016.

[34] ESRF and APS, X-ray oriented program, http://www.esrf.eu/Instrumentation/software/data-analysis/xop2.4, 2015.

[35] P. Phillips, Microwave separator for high energy particle beams, Rev. Sci. Instrum. **32**, 13 (1961).

[36] G. A. Loew and O. H. Altenmueller, Report No. SLAC PUB 135, 1965.

[37] H. Hahn and H. J. Halama, Design of the deflector for the rf beam separator at the brookhaven AGS, Rev. Sci. Instrum. **36**, 1788 (1965).

[38] D. Alesini, G. Di Pirro, L. Ficcadenti, A. Mostacci, L. Palumbo, J. Rosenzweig, and C. Vaccarezza, Rf deflector design and measurements for the longitudinal and transverse phase space characterization at SPARC, Nucl. Instrum. Methods Phys. Res., Sect. A **568**, 488 (2006).

[39] C. Behrens, F. J. Decker, Y. Ding, V. A. Dolgashev, J. Frisch, Z. Huang, P. Krejcik, H. Loos, A. Lutman, T. J. Maxwell, J. Turner, J. Wang, M. H. Wang, J. Welch, and J. Wu, Few-femtosecond time-resolved measurements of x-ray free-electron lasers, Nat. Commun. **5**, 3762 (2014).

[40] P. Craievich, M. Petronio, and S. G. Biedron, Implementation of radio-frequency deflecting devices for comprehensive high-energy electron beam diagnosis, IEEE Trans. Nucl. Sci. **62**, 210 (2015).

[41] T. Schietinger *et al.*, Commissioning experience and beam physics measurements at the SwissFEL injector test facility, Phys. Rev. Accel. Beams **19**, 100702 (2016).

[42] P. Emma, LBNL Technical Report No. NGLS-0020/ Addendum, 2013.

[43] R. Akre *et al.*, A transverse rf deflecting for bunch length, and phase space diagnostics, in *Proceedings of the 19th Particle Accelerator Conference, Chicago, IL, 2001* (IEEE, Piscataway, NJ, 2001).

[44] C. Sun, L. Doolittle, P. J. Emma, J. Jung, M. Placidi, and A. Ratti, Tuobno03, in *Proceedings of the 4th International Particle Accelerator Conference, IPAC-2013, Shanghai, China, 2013* (JACoW, Shanghai, China, 2013).

[45] T. Luo, D. Summers, and D. Li, Design of a normal-conducting RF-dipole deflecting cavity, in *Proceedings of the 4th International Particle Accelerator Conference, IPAC-2013, Shanghai, China, 2013* (Ref. [42]).